



The role of various etching time in Si nanostructures for ultra-high sensitivity photodetector

Anita S. Alber, Falah A.-H. Mutlak*

Department of Physics, College of Science, University of Baghdad, Baghdad, Iraq



ARTICLE INFO

Keywords:

Si nanostructure
Photo electrochemical etching
Ideality factor
Barrier height
Photodetector

ABSTRACT

The current study aimed to produce Si nanostructures ultra-high sensitivity photodetector by photo electrochemical method. The effect of changing some factors on the formation of porous silicon has been studied. The etching time has been changed using a photoelectrochemical procedure with a Halogen lamp. Relying on crystalline silicon n-type wafers (100) with resistivity of 0.1–100 Ω.cm, porous silicon layers were developed. Etching solution containing 16% HF was used at different etching times of (6, 9, 12, 15, 18, and 21) min. and 20 mA/cm² current density. The properties of the (J-V) and (Jph-V) in both darkness and photocurrent density, were used in demonstrating PS. When the crystal size is around a nanometer, XRD broadening of PS nanostructures increased as the crystallite size dropped, with the peaks becoming more widened. The peak of the PL spectrum changes a little on the high-energy side, indicating the presence of quantum confinement effect in porous silicon. While analyzing SEM data, the pores have cylindrical shape is a consequence of increasing the morphological characteristics average diameter. When compared to bulk silicon reflectivity, the observed significantly – lower PS surface Reflectance, demonstrated the porous silicon layer's thinness. In responsivity, two peaks appeared. The first one reaction peak was absorbed in the depletion region, at 500 nm of the Al-PS. While the second peak absorption was in the PS-c-Si depletion area at 500–600 nm and on 21 min etching time, where a maximum quantum efficiency of 83% was obtained.

1. Introduction

The PS first discovered by Uhlirs at Bell Laboratories by accident in the mid-1950s [1,2] and later by Turner [3]. Attempts to remove the top layers of crystalline silicon wafers in a process known as electropolishing or reverse plating resulted in the formation of porous silicon layers and deposited metal oxide on their surfaces [4–7]. The principal method for fabricating porous silicon layers has been electrochemical etching in an HF-based electrolyte [8–10]. Various quantum-size phenomena arise when the size of the Si wires size is a little less over a few nanometers, making PS even more exciting.

Because of its flexibility and adjustable properties, PS has become a popular material among scientists and technologists [11,12]. Over the last two decades, it has been used in a wide variety of sectors. The nanosized holes in crystalline silicon provide a sponge-like structure with pores and a crystalline silicon nanowire structure. The pore diameter, which can range from a few nanometers to a few microns depending on the formation factors, is used to classify PS. In comparison to bulk silicon, it has special electrical, chemical, and mechanical characteristics. PS has been shown to produce efficient visible light emission at room temperature [13–19]. PS can be made

* Corresponding author.

E-mail address: Falah.mutlak@sc.uobaghdad.edu.iq (F.A.-H. Mutlak).

by etching crystalline silicon in fluorine-based solutions chemically or electrochemically [20,21]. The drilling parameter, current density, HF concentration, Si chip type, resistance, and etching duration all influence PS attributes such porosity, refractive index, and pore diameter [22]. The PS possesses unique properties such as a higher ratio of surface/volume, a great nonporous structure, and a low index of refraction, all of which point to various possible uses such as filters, chemical sensors, and antireflection coatings in solar cells [23–26]. There are various techniques to formation PS can be used the Photoelectrochemical etching which consist HF solution is used to dissolve silicon wafers. Anodic current is applied to a silicon wafer in an HF electrolyte enclosed in a Teflon cell with light source. [27–33]. In this work, we use the photoelectrochemical etching process to create ultra-high sensitivity photodetector Si nanostructures. The structural, optical and electrical characteristics have been investigated.

2. Experimental details

PS samples have been produced by the photoelectrochemical etching (PECE) process. Fig. 1(A) represents the experiment setup for the PECE. The porous silicon was prepared by photoelectrochemical etching, we deposited aluminum film on the back side of silicon wafers n-type with a resistance of $(0.1\text{--}100)\ \Omega\text{ cm}$ in order to create an ohmic contact then we cut it to small pieces ($1 \times 1\text{ cm}^2$). After a piece was cut, the oxides were removed by rinsing in ethanol. An electrochemical cell composed of Teflon that etches a 1 cm^2 circular area on the wafer. The rubber O-ring is then placed between the Si wafer and the upper portion. The second one has a circular central hole of 1.3 cm^2 diameter to allow the solution to enter the Si wafer Fig. 1 placed into the etch cell with aluminum foil as the backside contact. The solution contains 16% HF and the rest is ethanol. To decrease the hydrogen bubbles, an absolute ethanol solution (99.9%) ($\text{C}_2\text{H}_5\text{OH}$) was used. Halogen lamp as light source was used with etching time (6, 9, 12, 15, 18, 21 min) and constant current density 20 mA/cm^2 . PS samples are shown in Fig. 1(B).

The voltage (J-V) characteristics of structural components (Al/PS/n-Si/Al) including both darkness and photocurrent density were investigated. A Halogen lamp was utilized to illuminate these samples at a variety of lighting power densities of (135, 170, 200, 210 and 250) mW/cm^2 with reverse voltages ranging from 6 to +6 V.

3. Results and discussion

The PS crystallite size was investigated using XRD, and the crystalline degree of etched samples was estimated using XRD Fig. 2. Bulk silicon's XRD results exhibits a very sharp peak. $2\theta = 69.92^\circ$ and show the wafer's single crystalline structure with altering full-width at half maximum (FWHM) for varying etching times (6, 9, 12, 15, 18, and 21) min and current density 20 Acm^2 , this peak gets very broad.

Table 1 Shows the crystallite sizes discovered in PS samples, which, when computed by using Scherrer equation, show a considerable decrease in crystallite size as etching time increases.

The SEM images of the PS structure that obtained for etching times (6, 9, 12, 15, 18 and 21) min with current density at 20 mA/cm^2 show in Fig. 3 we notice when the etching time is increased, the average pore diameter changes. The PS has a sponge-like structure with extensively branching pores, as seen in images.

The PL intensity increasing with increasing etching time, and the peak shifting to lower wavelength or high energy as shown in Fig. 4. The surface state of PL mechanism assumes that absorption of the carriers occurs in the silicon crystallites through quantum

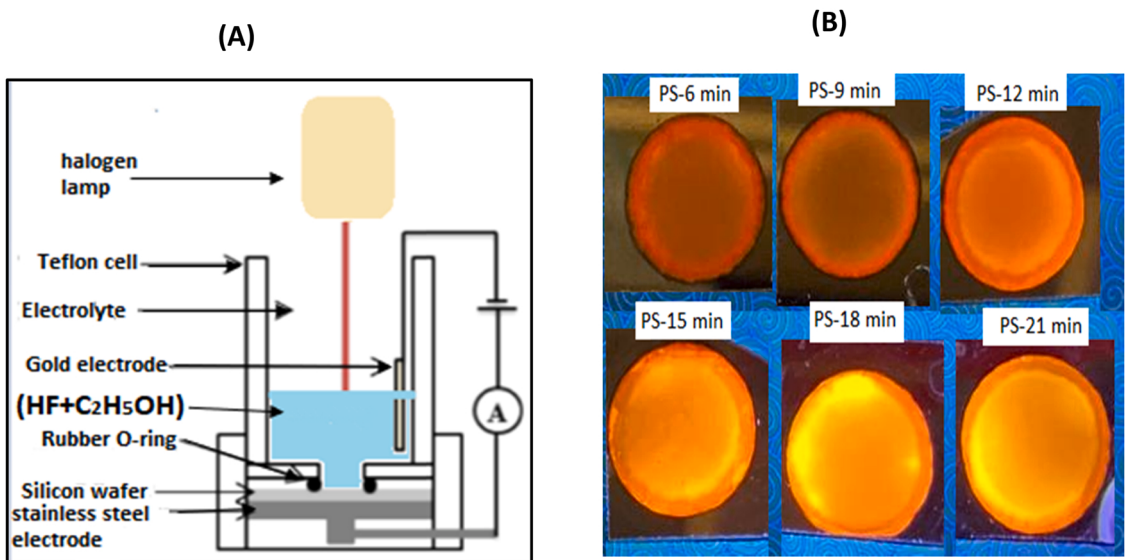


Fig. 1. (A) Schematic diagram of photoelectrochemical etching technique (B) Sample of PS prepared at different current densities.

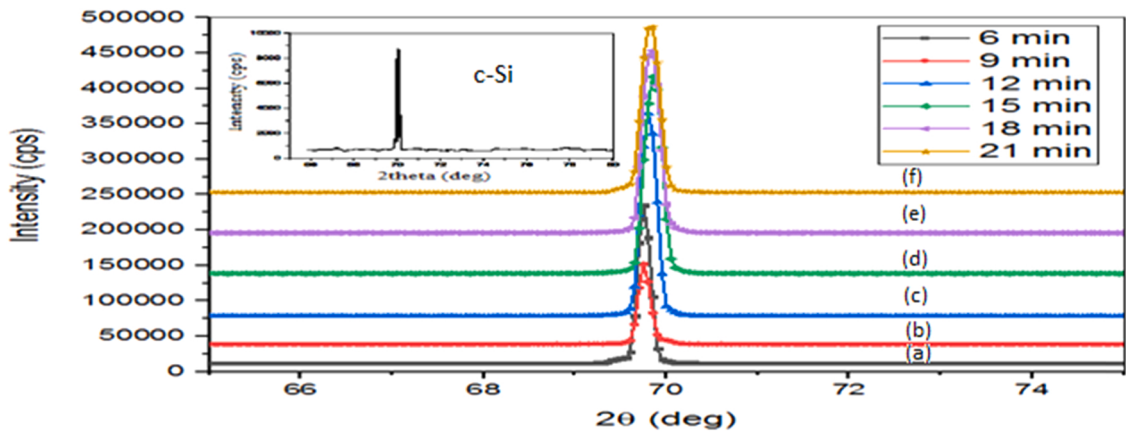


Fig. 2. XRD patterns of the c-Si (left) and PS with different etching time (a) 6 min, (b) 9 min, (c) 12 min, (d) 15 min, (e) 18 min and (f) 21 min, current density 20 mA/cm².

Table 1

Values obtained from measurements using XRD peaks for PS with various etching times.

Etching time	2θ (Deg.)	FWHM (Deg.)	d _{hkl} Exp. (Å)	C.S (nm)	hkl	Phase
6 min	69.8100	0.5000	1.3462	19.4	(400)	Hex. Cub.Si
9 min	69.8600	0.6000	1.3453	16.1	(400)	Hex. Cub.Si
12 min	69.8900	0.9500	1.3448	10.2	(400)	Hex. Cub.Si
15 min	69.8400	1.1200	1.3457	8.7	(400)	Hex. Cub.Si
18 min	69.8000	1.1000	1.3463	8.8	(400)	Hex. Cub.Si
21 min	69.9100	0.9500	1.3445	10.2	(400)	Hex. Cub.Si

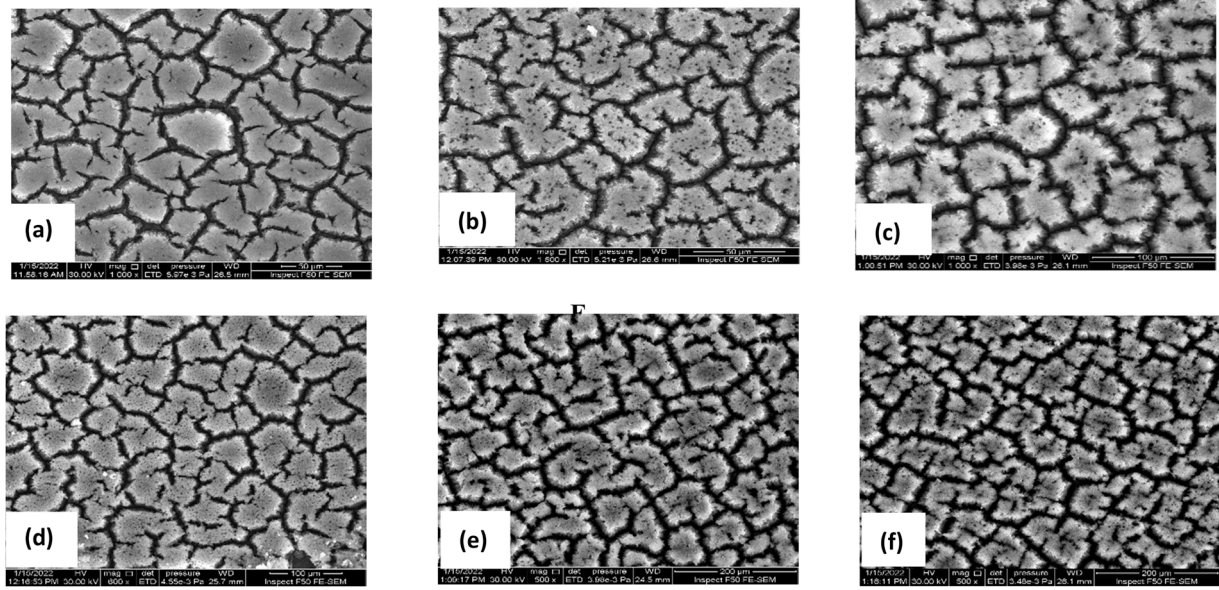


Fig. 3. SEM of PS prepared with different etching times (a) 6 min, (b) 9 min, (c) 12 min, (d) 15 min, (e) 18 min and (f) 21 min at current density 20 mA/cm².

confinement effects. The recombination centers are formed by silicon atoms at the surface of crystallite adjusting their bond lengths and angles to accommodate changes in local condition and the energy gap increasing in PS is due to confined of PS practical in a lower dimension, Hence, the probability of the recombination of electron and holes is a low dimensional structure and this agreement with the practical in a box theory. **Table 2**. The bandgap (Eg) increasing with increasing etching time using Eq. (1) and decreasing of wavelength due to the quantum confinement effect with decreasing of refractive index (n) Eq. (2) [34–36]. Clearly, the PL spectra

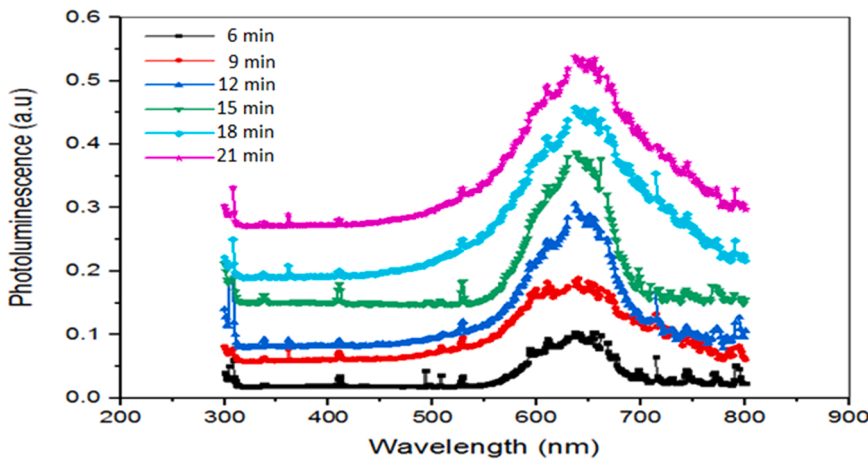


Fig. 4. PL spectra of PS at various etching times.

excitation value of 635 nm is visible, with a blue shift in the bandgap compared to bulk Si, which is attributable to the quantum confinement effect (QCE).

$$E = \frac{hc}{\lambda} \quad (1)$$

$$n = \sqrt{1 + \frac{A}{B + E_g}} \quad (2)$$

where A = 13.6 eV, B = 3.4 ev, h: Plank constant c: speed of light.

Fig. 5 shows the reflection spectra of the PS compared to the c-Si sample. The Measurement of R% of PS layers showed that we can greatly reduce surface reflectivity on crystalline Si wafers by forming a thin PS layer by anodization etching. These results show that a porous surface layer on crystalline silicon actually improves performance by acting as an ARC layer. Si bulk has a high reflectance when the roughness of the PS layers is enhanced. This could be linked to the development of many layers of pores, which is thought to enhance pore diameter. Moreover, the larger the pores' diameter, the more effective they are as showed in **Fig. 5(f)**.

PS electrical measurements imply a current density - voltage analysis (J-V). PS etching structure at various times. J-V measurements were performed in a dark closed box at room temperature. By applying a DC voltage to forward and reverse bias (from-6-6), the J-V characteristic can be determined. The J-V measurements for PS layers prepared at etching times (6, 9, 12, 15, 18 and 21) min with current density at 20 mA/cm² and 16% HF concentration. PS layers have inhomogeneous distribution and sizes of pores, resulting in variable porosity, which is determined by the porosity attribute. **Fig. 6** comparing the properties of two biases exhibit rectifying behavior, which could be linked to the creation of an isotope hetero-junction [37].

This phenomenon is explained by changes in their energy gaps, which is crucial in explaining the rise in resistivity once the PS layer is generated. The high value is owing to the difference in charge carrier depletion in PS versus c-Si due to PS's larger band-gap, which is related to the recombination process. [38]. for c-Si, PS, and varied etching times under dark, log (J) by bias voltage. apply biases and reverse voltage in the – 6 to + 6 V range, **Fig. 7** As the etching time increases, the output current drops due to growing resistivity (of c-Si and PS) and thickness of the PS layer [39].

Table 3 Show that J-V measurements can be used to estimate the electrical properties of bulk silicon and pores silicon, such as ideality factor (n) and barrier height (Φ_{Bn}) The saturation current density J_s is obtained by extrapolating the linear section of the semi-log forward I-V curves to zero applied voltage, and the Φ_{Bn} values are determined using formulae [40].

$$n = \frac{q}{k_B T} \frac{dV}{d(\ln J)} \quad (3)$$

Table 2
Values obtained from PL peaks PS with different etching time.

Etching time	λ (nm)	E_g (ev)	n
6 min	640.1	1.9371	1.8836
9 min	635.8	1.9502	1.8820
12 min	634.9	1.9530	1.8814
15 min	634.3	1.9592	1.8809
18 min	631.8	1.9626	1.8804
21 min	630.1	1.9682	1.8797

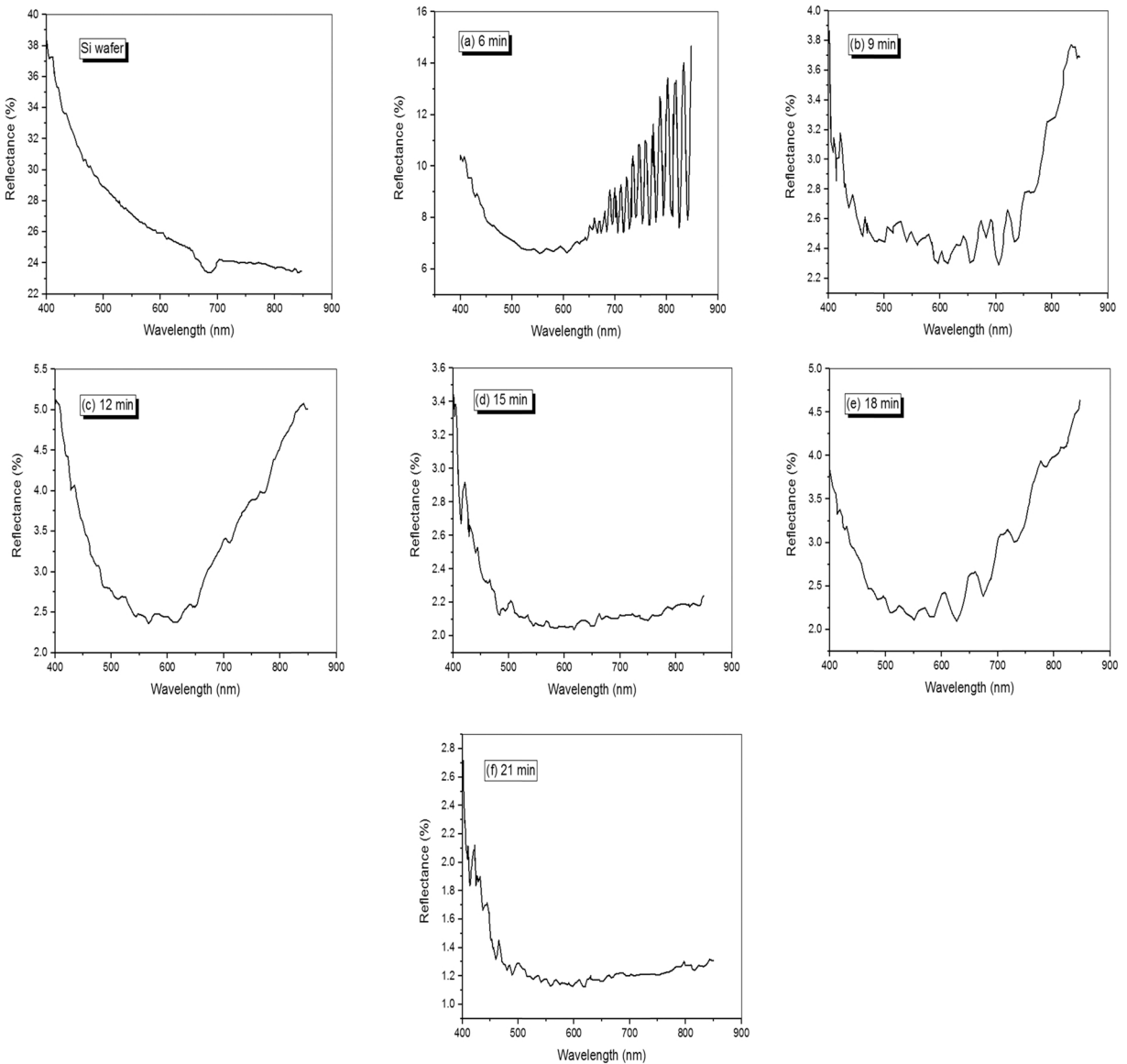


Fig. 5. Reflectivity spectra of c-Si and PS samples with different etching time (a) 6 min, (b) 9 min, (c) 12 min, (d) 15 min, (e) 18 min and (f) 21 min, current density 20 mA/cm^2 .

$$\Phi_{Bn} = \frac{k_B T}{q} \ln \left(\frac{A^{**} T^2}{J} \right) \quad (4)$$

J : forward current density ($\mu\text{A}/\text{cm}^2$), k_B : Boltzmann constant ($1.38 \times 10^{-23} \text{ J/K}$), V : the applied voltage, A^{**} : represents the value of Richardson's constant ($\text{A}/\text{cm}^2\text{K}$).

Because the distance between the depletion zone and the photo-current is increased, the photo-current is constantly in the reverse-biased direction. The intrinsic electric field widens as the reverse bias voltage rises, increasing the likelihood of split electron-hole pairs, as seen in Fig. 8.

The spectral responsivity is an important parameter to determine the spectral performance range of photodetector. Fig. 9 shows the responsivity as a function of wavelength for Al/PS/n-Si/Al samples fabricated at different etching times and etched at 20 mA/cm^2 current density with 16% HF concentration. The spectral responsivity curve includes two regions; the first region illustrates higher responsivity due to the absorption of visible light (500–600 nm) by PS. The second region corresponds to the IR absorption (800–900 nm) with c-Si layer. After that the reduction in the responsivity is observed that attributed to the absorption of light by silicon substrate. The sample prepared at 21 min shows higher responsivity reached 0.004 A/W compared with 0.001 A/W for that prepared at 6 min. This is related to high roughness surface which leads to increase in the photon absorption and photocurrent.

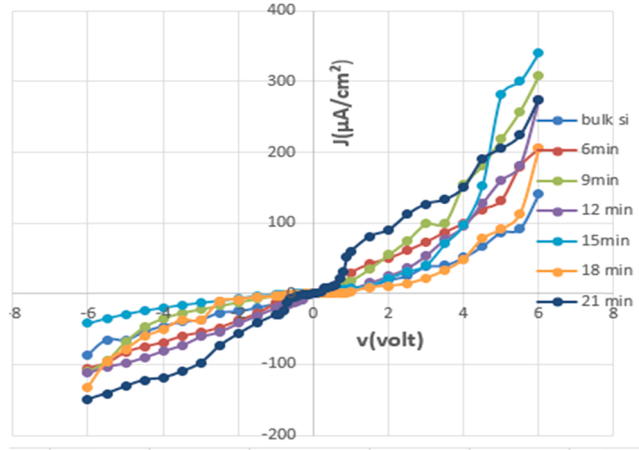


Fig. 6. (J-V) characteristics of c-Si and PS prepared at various etching time (6, 9,12,15,18 and 21) min and current density 20 mA/cm^2 .

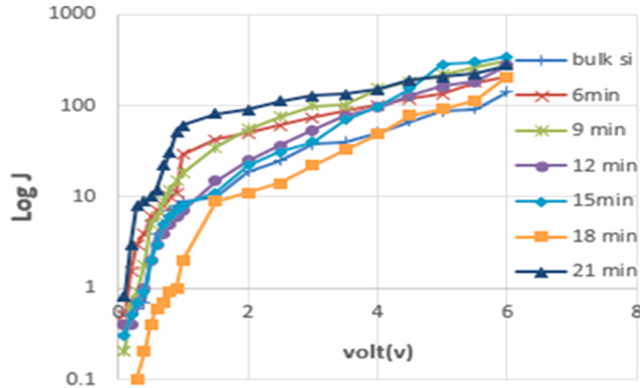


Fig. 7. $\log(J)$ by bias voltage under dark for c-Si and PS prepared at different etching times (6, 9,12,15,18 and 21) min and current density 20 mA/cm^2 .

Table 3

Values obtained from experiments of bulk Si and PS the values (n), (J_s) and (Φ_{Bn}).

Sample	Slop	n	$J_s (\mu\text{A}/\text{cm}^2)$	$\Phi_{Bn} (\text{eV})$
Bulk Si	0.048562	1.874478	25	0.6914
PS-6 min	0.059854	2.310377	29	0.6876
PS-9 min	0.063341	2.444961	18	0.6999
PS-12 min	0.072926	2.814957	15	0.7046
PS-15 min	0.081713	3.154114	11	0.7126
PS-18 min	0.087397	3.373527	10	0.715
PS-21 min	0.089653	3.460594	25	0.6914

Furthermore, the responsivity curve is shifted toward the visible region due to reduction in the energy gap. The responsivity is determined by using Eq. (5) [41].

$$R_\lambda = \frac{I_{ph}}{P_{in}} \quad (5)$$

I_{ph} is the current of the optical container, the P_{in} is the input power, and Spectral responsivity R_λ is the detector signal that will be obtainable for enforcement.

Fig. 10 displays the detectivity measuring and it was found that specimens have high values. The dark current was small which indicating a lower noise to indication rate leads to better detection with an increase of etched time of PS the specific detectivity values, that are in the range of $(0.1\text{--}0.4) \times 10^{12} (\text{cm} \cdot \text{Hz}^{1/2} / \text{W})$ at 800 nm and $(0.04\text{--}0.11) \times 10^{12} (\text{cm} \cdot \text{Hz}^{1/2} / \text{W})$ at 600 nm. The Eq. (6) is used to compute detectivity [42,43].

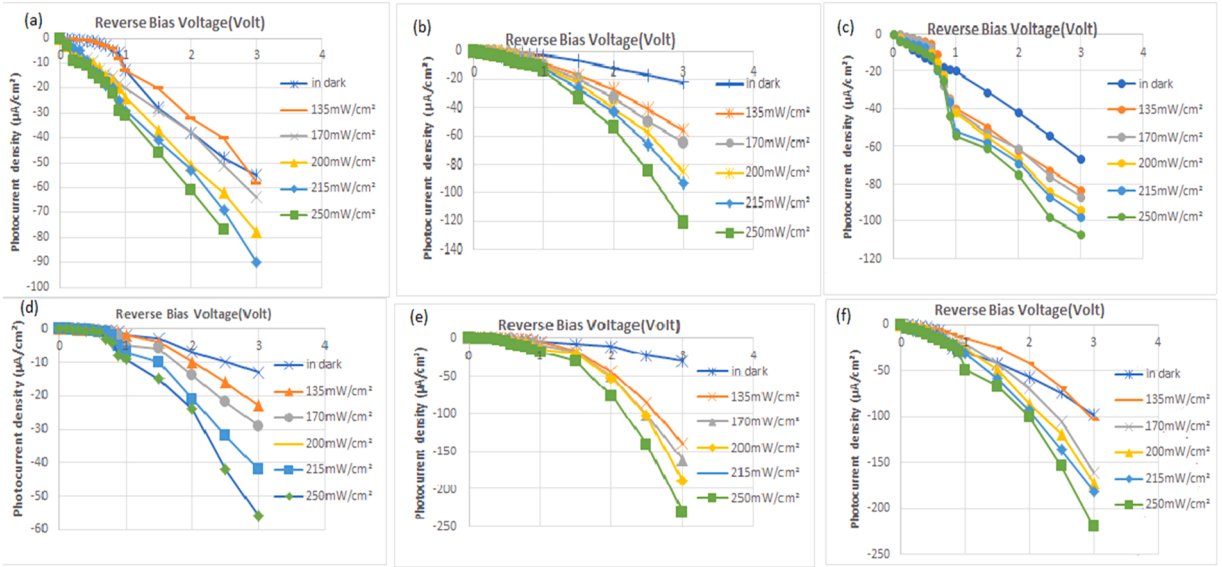


Fig. 8. I_{ph} -V characteristic under illumination of PS prepared at different etching times (a) 6 min, (b) 9 min, (c) 12 min, (d) 15 min (e) 18 min and (f) 21 min, current density $20 \text{ mA}/\text{cm}^2$.

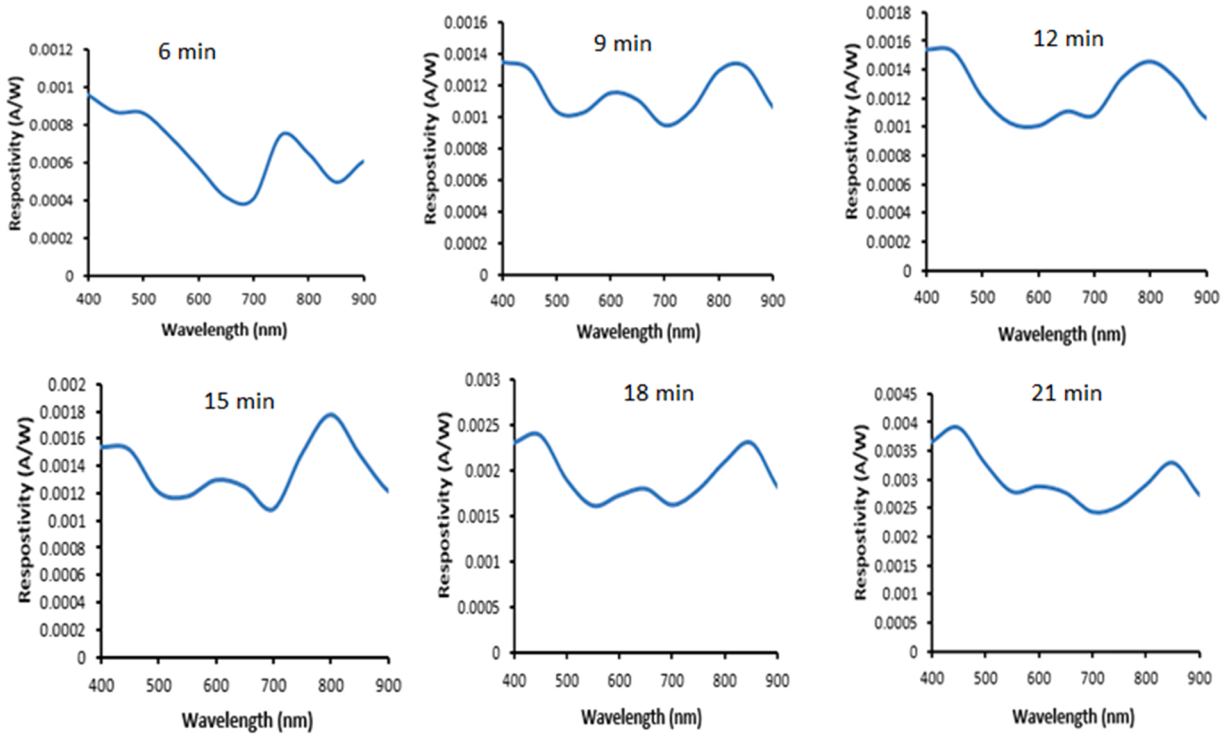


Fig. 9. Responsivity of Al/PS/n-Si/Al samples prepared at different etching times.

$$D^* = \frac{\sqrt{S_{det} \Delta f}}{NED} \quad (6)$$

When the detectivity (D^*), represents the response of the frequency ($\Delta f = 1/2\pi\tau$), detector active area (S_{det}), represents the noise equivalent power (NEP).

Quantum efficiency (Q.E) was achieved in the spectral region (400–900 nm). Fig. 11 illustrates the Quantum efficiency of Al/PS/n-Si/Al samples prepared at different etching times. The quantum efficiency is directly related to the spectral responsivity and estimated

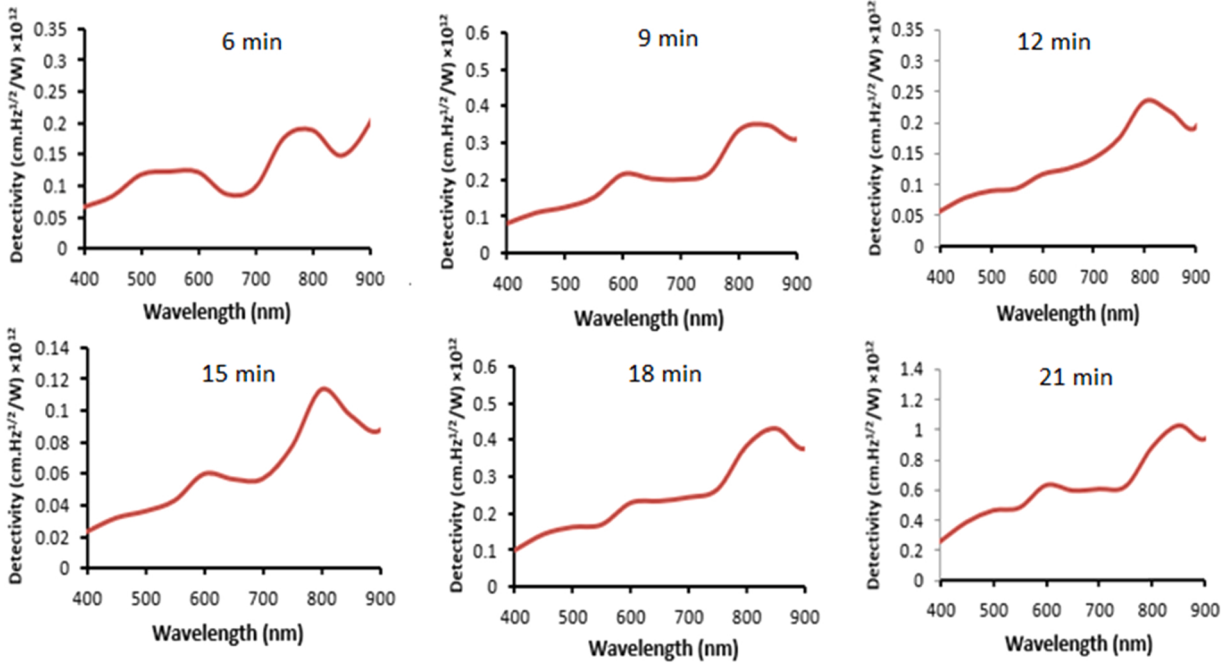


Fig. 10. Detectivity of Al/PS/n-Si/Al samples prepared at different etching times.

from Eq. (7). The value of quantum efficiency is increased from 18.54% to 83.12% with increased etching time that used to prepare PS. This is attributed to the same reason mentioned for the responsivity [44,45].

$$\eta = \frac{h\nu}{q} R_\lambda \quad (7)$$

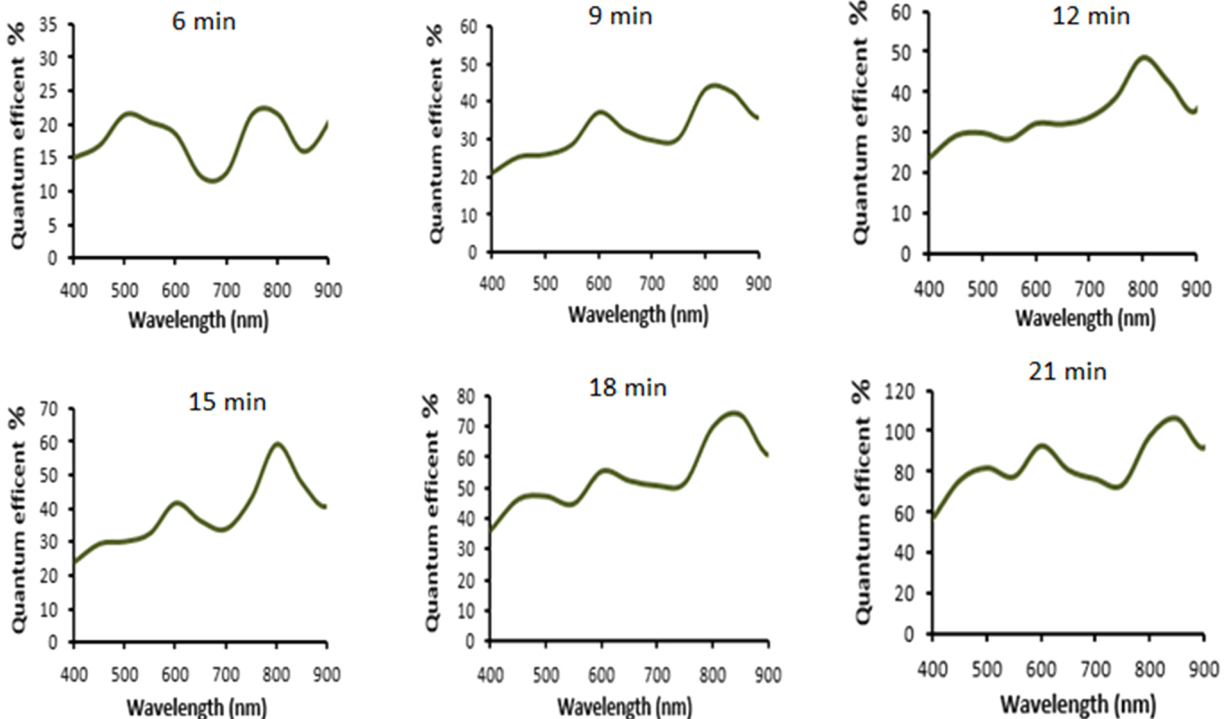


Fig. 11. Quantum efficiency of Al/PS/n-Si/Al samples prepared at different etching times.

where: η is the Quantum efficient, h the Plank constant, v stands for the frequency of photon.

4. Conclusions

The influence of varied etching time intervals (6, 9, 12, 15, 18, and 21) min on formation of Porous Silicon (PS) via PECE was investigated. The results of PS show the nanostructure (mesoporous silicon) formed, with decreasing pore diameter from 52.34 nm to 28.21 nm with increasing etching time. PS has sponge like structure and the pore diameter is reduced with increased etching time which leads to decreases PS resistivity and increase the current pass through PS layer. The Al/PS/n-Si/Al photodetector shows two response peaks one at visible region and other at IR region. Also, Al/PS/n-Si/Al photodetector of PS prepared at 21 min shows high responsivity, detectivity and quantum efficiency compared with that prepared at 6 min etching time. This is due to high roughness, low reflectivity, and high photocurrent of this nanostructure. The surface morphology of the PS layer is discovered to be dependent on fabrication conditions. As a result, time shifting can be utilized to regulate the final structure's size and shape.

Declaration of Competing Interest

Authors would like to declare that they do not have any conflict of interests.

References

- [1] A. Uhlig, Electrolytic shaping of germanium and silicon, *Bell Syst. Tech. J.* 35 (2) (1956).
- [2] A. Uhlig, I.W. Uhlig, Historical perspective on the discovery of porous silicon, *Phys. Status Solidi C Conf. Crit. Rev.* 2 (9) (2005) 3185–3187.
- [3] D. Turner, Electropolishing silicon in hydrofluoric acid solutions, *Electrochem. Soc.* 105 (7) (1958).
- [4] H. Abid, U. Nayef, F. Mutlak, Preparation and characterization Co₃O₄ nanoparticles on porous silicon for humidity sensor by photoluminescence, *Optik* 178 (2019).
- [5] S. Khudiar, U. Nayef, F. Mutlak, S. Abdulridh, Characterization of NO₂ gas sensing for ZnO nanostructure grown hydrothermally on porous silicon, *Optik* 249 (2022), 168300.
- [6] Duha H. Jwied, Uday M. Nayef, Falah A.H. Mutlak, Synthesis of C:Se nanoparticles via laser ablated with magnetic field on porous silicon for gas sensor applications, *Optik* 242 (2021), 167207, <https://doi.org/10.1016/j.jleo.2021.167207>.
- [7] S. Khudiar, U. Nayef, F. Mutlak, Preparation and characterization of ZnO nanoparticles via laser ablation for sensing NO₂ gas, *Optik* 246 (2021), 167762, <https://doi.org/10.1016/j.jleo.2021.167762>.
- [8] L. Canham, *Properties of Porous Silicon*, The Institution of Electrical Engineers, London, 1997.
- [9] V. Lehmann, *Electrochemistry of Silicon Instrumentation, Science, Materials and Applications*, Wiley-VCH, Germany, 2002, <https://doi.org/10.1002/3527600272>.
- [10] Z.C. Feng, R. Tsu, *Porous Silicon*, Singapore World Scientific, 1994.
- [11] A. Pap, Investigation of Pristine and Oxidized Porous Silicon (Ph.D. thesis), Faculty of Technology, Department of Electrical and Information Engineering, infotech Oulu, University of Oulu, 2005.
- [12] V. Dona, C. Curtis, G. Credo, M. Sailor, R. Penner, Enhanced luminescence and optical cavity modes from uniformly etched porous silicon, *Silicon-Based Optoelectron. Mater.* 298 (1993) 185–191.
- [13] S. Tamulevicius, A. Guobiene, V. Grigaliunas, Fabrication of PS microstructures using electrochemical, *Mater. Sci. J.* 9 (4) (2003).
- [14] F. Mutlak, N. Harab, Effect of etching current density on spectroscopic, structural and electrical properties of porous silicon photodetector, *Opt. Int. J.* 249 (2021), 168298.
- [15] S. Adachi, T. Kubota, Electroluminescence from porous silicon formed by photoetching in an HF/I2 solution, *J. Porous Mater.* 15 (2008) 427–431.
- [16] A. Abd-Alghafoor, Z. Hassan, K. Omar, Laser-induced etching parameters impact on optical properties of the silicon nanostructures, *Sci. China Technol. Sci.* 54 (1) (2011) 58–62.
- [17] C. Vinegoni, M. Cazzanelli, L. Pavesi, Porous silicon microcavities, *Silicon-Based Mater. Devices* 2 (2001) 123–192.
- [18] L. Yongfu, Radial microstructure and optical properties of a porous silicon layer by pulse anodic etching, *J. Semicond.* 32 (4) (2011) 1–4.
- [19] I. Tiginianu, S. Langa, H. Foell, V. Ursachi, *Porous III-V Semiconductors*, 2009.
- [20] H. Abood, F. Mutlak, Structural, morphological and optical properties of n-type porous silicon-effect of etching current density, *IOP Conf. Ser. Mater. Sci. Eng.* 757 (2020), 012065.
- [21] H. Foll, M. Christoffersen, J. Caestensen, G. Hasse, Formation and application of porous silicon, *Mater. Sci. Eng.* 39 (4) (2002) 93–141.
- [22] D. Blackwood, Y. Zhang, Porous silicon: influence of etching temperature on microstructure and luminescence, *Surf. Rev. Lett.* 8 (5) (2001) 429–433.
- [23] R. Žvalionienė, J. Waluk, I. Čevas, Photoluminescence properties of porous silicon with CdSe/ZnS quantum dots, *Mater. Sci.* 17 (3) (2011) 232–235.
- [24] N. Harb, F. Mutlak, Production and characterization of porous silicon via laser-assisted etching: Effect of gamma irradiation, *Optik* 246 (2021), 167800.
- [25] A. Ahmed, M. Abdulameer, M. Kadhim, F. Mutlak, Plasma parameters of Au nano-particles ablated on porous silicon produced via Nd-YAG laser at 355 nm for sensing NH₃ gas, *Optik* 249 (2022), 168260.
- [26] F. Mutlak, A. Ahmed, U. Nayef, Q. Al-zaidi, S. Abdulridha, Improvement of absorption light of laser texturing on silicon surface for optoelectronic application, *Optik* 237 (2021), 166755, <https://doi.org/10.1016/j.jleo.2021.166755>.
- [27] P. Kumar, Effect of silicon crystal size on photoluminescence appearance in porous silicon, *Int. Sch. Res. Netw. ISRN Nanotechnol.* 2011 (2011) 1–6, 163168.
- [28] M. Jayachandran, M. Paramasivam, K. Murali, D. Trivedi, M. Raghavan, Synthesis of porous silicon nanostructures for photoluminescent devices, *Mater. Phys. Mech.* 4 (2001) 143–147.
- [29] M. Eddowes, Anodic dissolution of p- and n-type silicon: Kinetic study of the chemical mechanism, *J. Electroanal. Chem.* 280 (2) (1990).
- [30] R. Smith, S. Collins, Porous silicon formation mechanisms, *J. Appl. Phys.* 71 (1992) R1–R22.
- [31] B. Xavier, *Electrochemically Etched Pore Arrays in Silicon for X-Ray Imaging Detectors* (Ph.D. dissertation), KTH, 2005.
- [32] B. Sukumar, J. Kanungo, *Nanocrystalline porous silicon: Crystalline Silicon-Properties and Uses*, InTech, 2011.
- [33] V. Doan, R. Penner, M. Sailor, Enhanced photoemission from short wavelength photochemically etched porous silicon, *J. Phys. Chem.* 97 (17) (1993) 4505–4508.
- [34] M. Kadhim, Preparation and Characterization of Photovoltaic Properties of Porous Silicon (Thesis), College of Engineering, Nahrain University, 2017, pp. 1034–1039.
- [35] S. Lazarouk, P. Jagurio, G. Maiello, S. La Monica, G. Masini, E. Proverbio, A. Ferrari, Visual determination of thickness and porosity of porous silicon layers, *Thin Solid Films* 297 (1–2) (1997) 97–101.
- [36] F. Mutlak, R. Jamal, A. Ahmed, Pulsed laser deposition of TiO₂ nanostructures for verify the linear and non-linear optical characteristics, *IJS* 62 (2021) 2.
- [37] A. Alwan, The effect of thermal oxidation time on the structure and influence on optical properties for porous silicon prepared by photo electrochemical etching, *Eng. Technol. J.* 27 (4) (2009) 727–735.

- [38] A. Acevedo, Solar Cells - Research and Application Perspectives 2711, In Tech, 2013.
- [39] G. Algün, M. Arıkan, An investigation of electrical properties of porous silicon, *Turk. J. Phys.* 23 (4) (1999) 789–798.
- [40] E. Rhoderick, R. Williams, Metal-Semiconductor Contacts, second ed., Clarendon, 1988, pp. 1–225.
- [41] M. Sailor, J. Heinrich, J. Lauerhaas, Luminescent porous silicon: synthesis, chemistry, and applications. *Studies in Surface Science and Catalysis*, Elsevier, 1997, pp. 209–235.
- [42] D. Jwied, U. Nayef, F. Mutlak, Preparation and characterization of C: Se nano-rods ablated on porous silicon, *Opt. Int. J. Light Electron Opt.* 239 (2021), 166811.
- [43] S. Khudiar, F. Mutlak, U. Nayef, Synthesis of ZnO nanostructures by hydrothermal method deposited on porous silicon for photo-conversion application, *Optik* 247 (2021), 167903.
- [44] A. Ahmed, W. Yaseen, Q. Abbas, F. Mutlak, Plasma treatment effect on SnO₂-GO nano-heterojunction: fabrication, characterization and optoelectronic applications, *Appl. Phys. A* 127 (746) (2021).
- [45] D. Jwied, U. Nayef, F. Mutlak, Improvement of responsivity of C:Se nanoparticles ablated on porous silicon, *Optik* 241 (2021), 167222.